



Performance of bifunctional CuO–CeO₂/γ-Al₂O₃ catalyst in dimethoxymethane steam reforming to hydrogen-rich gas for fuel cell feeding



A.A. Pechenkin^{a,b}, S.D. Badmaev^{a,b}, V.D. Belyaev^{a,b}, V.A. Sobyenin^{a,*}

^a Boreskov Institute of Catalysis, Pr. Lavrentieva, 5, Novosibirsk 630090, Russia

^b Novosibirsk State University, Pirogova St., 2, Novosibirsk 630090, Russia

ARTICLE INFO

Article history:

Received 15 September 2014

Received in revised form 1 December 2014

Accepted 3 December 2014

Available online 5 December 2014

Keywords:

Hydrogen

Dimethoxymethane

Dimethyl ether

Methanol

Copper–ceria–alumina

ABSTRACT

Dimethoxymethane steam reforming (DMM SR) to hydrogen-rich gas over a bifunctional CuO–CeO₂/γ-Al₂O₃ catalyst was studied. The performance of γ-Al₂O₃, CeO₂/γ-Al₂O₃, and CuO/γ-Al₂O₃ under DMM SR conditions was studied as well to elucidate the role of each catalyst component. BET, TPR, FTIR spectroscopy, XRD, TEM, EDXA and HAADF-STEM techniques were used for catalyst characterization. Complete DMM conversion was observed over the CuO–CeO₂/γ-Al₂O₃ catalyst under atmospheric pressure, $T = 300\text{ }^{\circ}\text{C}$, GHSV = 10,000 h^{−1} and H₂O/DMM = 5 mol/mol with hydrogen productivity of 15.5 L H₂/(g_{cat}·h) and CO content in the hydrogen-rich gas below the equilibrium value. DMM SR proceeds via a consecutive two-step reaction mechanism including DMM hydration to methanol and formaldehyde on γ-Al₂O₃ acid sites and steam reforming of the formed methanol and formaldehyde to hydrogen-rich gas on alumina-supported mixed copper–cerium oxide species. The CuO–CeO₂/γ-Al₂O₃ catalyst proved to be highly promising for multi-fuel processor approach: steam reforming of DMM, dimethyl ether and methanol on the same catalyst under similar reaction conditions to hydrogen-rich gas for fuel cell feeding.

© 2014 Elsevier B.V. All rights reserved.

1. Introduction

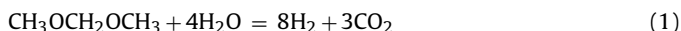
Power units based on low- and high-temperature (LT and HT) polymer electrolyte membrane fuel cells (PEMFC) are considered as alternative environmentally sound sources of electricity [1–5]. PEMFCs are fuelled by hydrogen, which is usually generated by catalytic steam reforming (SR) of hydrocarbons or oxygenated organic compounds to produce synthesis gas, which is then upgraded to hydrogen-rich gas with low CO content.

Generation of hydrogen-rich gas for PEMFC feed applications from synthetic oxygenated organic compounds, such as methanol and dimethyl ether (DME), attracts attention of scientists for a long time [1–16]. It has been shown that methanol and DME, in contrast to hydrocarbons, can be converted easily and selectively to hydrogen-rich gas at relatively low temperatures (250–350 °C). Efficient methanol and DME SR catalysts have been proposed. They made it possible to design catalytic “fuel processors” – generators of hydrogen-rich gas.

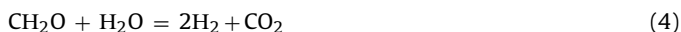
Similarly to methanol and DME, dimethoxymethane (DMM) is an easy to synthesize oxygenated compound of C₁ chemistry. DMM is generally produced by condensation of methanol with formaldehyde. Direct catalytic oxidation of methanol to DMM is under development now [17]. Under normal conditions, DMM is a liquid. Therefore, it can be easily stored and transported. It is worth emphasizing that DMM is a noncorrosive, nontoxic material with a wide scope of applications [18]. It is used as unique powerful solvent for aerosols, pump sprays in pharmaceutical and perfume industries [19]. DMM selective oxidation is a new alternative for the production of highly concentrated formaldehyde [20]. Direct DMM PEMFCs are being developed now, although they are still less efficient than PEM FC fuelled by hydrogen [21]. DMM can be used as an additive to diesel fuel to improve combustion and reduce pollutant emissions of diesel engines [22]. Note again that DMM, in contrast to highly toxic methanol, is an environmentally benign chemical that is of key importance for household and portable fuel cell applications. These facts together with the recent data on DMM SR reported in [23–26] predict increased DMM demand that will become a promising feedstock for production of hydrogen-rich gas for PEM FC feeding.

* Corresponding author.

Catalytic steam reforming of DMM is one of the most efficient methods for production of hydrogen-rich gas:



DMM SR studies are still at an early stage. Only several papers have been published [23–26]. It has been shown that the reaction proceeds via a consecutive two-step mechanism including DMM hydration to methanol and formaldehyde (2), followed by steam reforming of the formed methanol (3) and formaldehyde (4) to hydrogen-rich gas:



Note that the DMM SR reaction mechanism is inherently similar to that of DME SR. According to [10–16], DME SR also proceeds via a consecutive two-step reaction mechanism including DME hydration to methanol, followed by methanol SR to hydrogen-rich gas.

Carbon monoxide can be also formed during DME SR [10–16] and DMM SR [23–26], for example, by reverse water-gas shift reaction:



In [23–25] DMM SR was performed using mechanically mixed catalytic systems comprised of a solid acid catalyst for DMM hydration and a Cu-based catalyst for methanol/formaldehyde SR. The systems showed good performance and, depending on the catalyst compositions, provided for complete DMM conversion and H_2 productivity of 1.2–7.4 L $\text{H}_2/(\text{g}_{\text{cat}} \text{ h})$ at 250–300 °C. However, for mechanically mixed catalysts it is difficult to prepare a uniformly mixed catalyst bed that does not disintegrate into components during reaction. Recently, efficient bifunctional $\text{CuO-CeO}_2/\gamma\text{-Al}_2\text{O}_3$ catalysts have been suggested for DMM SR [26]. These catalysts contain both the surface acid sites of $\gamma\text{-Al}_2\text{O}_3$ for DMM hydration and Cu-based species for methanol/formaldehyde SR. According to [13,14], $\text{CuO-CeO}_2/\gamma\text{-Al}_2\text{O}_3$ catalysts are active for methanol and DME SR as well. It was shown that DME hydration proceeds on the acid sites of $\gamma\text{-Al}_2\text{O}_3$, whereas methanol SR is catalyzed by alumina-supported mixed copper–cerium oxide species CuO-CeO_2 (which most likely consist of a solid solution of copper ions in ceria).

The present work reports the results of studies on DMM SR to hydrogen-rich gas over the most efficient bifunctional catalyst 10 wt.% $\text{CuO-5 wt.\% CeO}_2/\gamma\text{-Al}_2\text{O}_3$. The catalyst was characterized by BET, TPR, XDR, FTIR spectroscopy, TEM, EDXA and HAADF-STEM techniques. To elucidate the role of each catalyst component in DMM SR reaction, the data on the catalytic performance of $\gamma\text{-Al}_2\text{O}_3$, 5 wt.% $\text{CeO}_2/\gamma\text{-Al}_2\text{O}_3$, and 10 wt.% $\text{CuO}/\gamma\text{-Al}_2\text{O}_3$ are presented as well. Based on the data on DME SR and methanol SR over 10 wt.% $\text{CuO-5 wt.\% CeO}_2/\gamma\text{-Al}_2\text{O}_3$ catalyst the feasibility of developing a multi-fuel processor for generating hydrogen-rich gas from DMM, DME and methanol for PEMFC feeding applications is considered.

2. Experimental

2.1. Catalyst preparation

10 wt.% $\text{CuO-5 wt.\% CeO}_2/\gamma\text{-Al}_2\text{O}_3$ catalyst sample was prepared by incipient wetness co-impregnation of $\gamma\text{-Al}_2\text{O}_3$ ($S_{\text{BET}} = 200 \text{ m}^2/\text{g}$, $V_{\text{pore}} = 0.7 \text{ cm}^3/\text{g}$, granule diameter 0.25–0.5 mm) with aqueous solutions of copper (II) and cerium (III) nitrates taken at the desired ratio. 10 wt.% $\text{CuO}/\gamma\text{-Al}_2\text{O}_3$ and 5 wt.% $\text{CeO}_2/\gamma\text{-Al}_2\text{O}_3$ catalyst samples were prepared by incipient wetness impregnation of the $\gamma\text{-Al}_2\text{O}_3$ with aqueous solutions of copper (II) and cerium

(III) nitrates, respectively. The samples were dried at 100 °C in air and calcined at 400 °C–500 °C for 3 h in air. The catalysts are denoted hereinafter as $\text{CuO-CeO}_2/\gamma\text{-Al}_2\text{O}_3$, $\text{CuO}/\gamma\text{-Al}_2\text{O}_3$, and $\text{CeO}_2/\gamma\text{-Al}_2\text{O}_3$. $\gamma\text{-Al}_2\text{O}_3$ was provided by JSC Katalizator, Novosibirsk, Russia, and was calcined at 500 °C for 4 h in air before being used as the support.

2.2. Catalyst characterization

Actual CuO and CeO_2 loadings in the catalysts were determined by inductively coupled plasma atomic emission spectrometry (Optima instrument; Perkin-Elmer). The specific BET surface areas (S_{BET}) of the support and the catalysts were determined from the nitrogen adsorption isotherms at –196 °C using a TriStar 3000 apparatus.

Temperature-programmed reduction (TPR) experiments were carried out using a STA 409 PC Luxx derivatograph fitted with a QMS-200 mass spectrometer. The samples (~50 mg) were heated from room temperature to 400 °C (5 °C/min) in a 5 vol.% $\text{H}_2\text{-Ar}$ mixture flowing at 140 mL/min.

FTIR spectroscopy (Shimadzu FTIR-8300 spectrometer) was applied to determine the acidity of the catalysts by monitoring low-temperature CO adsorption according to the procedure described in [27,28]. The catalysts were reduced and degassed in the IR cell at 400 °C, cooled to –173 °C and treated with doses of CO from 0.1 to 10 torr. The used procedure makes it possible to determine both the amount and strength of Brønsted acid sites (BAS) and Lewis acid sites (LAS), which exhibit adsorption bonds at 2150–2175 cm^{-1} and 2180–2240 cm^{-1} , respectively.

X-ray diffraction (XRD) patterns of the catalysts were recorded on a URD-63 diffractometer ($\text{CuK}\alpha$ radiation; graphite monochromator). The scanning range was 20–80° (2 θ) with a step of 0.02° (2 θ) and sampling time of 1.0 s. The diffraction data were processed using the PowderCell 2.4 programme yielding the phase composition, lattice parameters, and the size of coherent-scattering regions (CSR) of the samples. Data from the JCPDS international diffraction database were used as a reference.

Transmission electron microscopy (TEM) images and energy-dispersive X-ray (EDX) chemical microanalysis patterns of the catalysts were obtained using a JEM 2010 electron microscope (JEOL, 0.14 nm resolution at 200 kV) coupled with an EDX spectrometer (EDAX Co., Si(Li) detector with 130 eV energy resolution).

The analysis of the surface composition and compositional homogeneity of the supported particles in the catalyst was performed using a high-angle annular dark-field scanning TEM (HAADF-STEM) technique. The photographs and maps were taken on a 200 kV JEOL 2200FS TEM/STEM. The microscope was equipped with a HAADF-detector to obtain images of high atomic contrast in scanning mode, and with an EDX-analyzer for local microanalysis and EDX-local mapping.

2.3. Catalyst testing

DMM, methanol and DME steam reforming reactions were carried out in a U-shaped fixed-bed continuous-flow reactor (i.d. 4 mm) at 150–380 °C under atmospheric pressure. All the catalysts (particle size of 0.25–0.5 mm) were pre-reduced in situ at 300 °C for 1 h using 5 vol.% H_2 in N_2 . Then the temperature was lowered to 150–200 °C in flowing H_2 , and the catalysts were exposed to the feed composed of (vol.%) 14 DMM, 70 H_2O and 16 N_2 (for DMM SR); 40 methanol, 40 H_2O and 20 N_2 (for methanol SR) or 20 DME, 60 H_2O and 20 N_2 (for DME SR). The total gas hourly space velocity (GHSV) was 10,000 h^{-1} . The compositions of the inlet and outlet gas mixtures were analyzed by a gas chromatograph (GC Chromos-1000) equipped with TCD/FID detectors and Porapack T/molecular sieve (CaA) columns. Argon was used as a carrier gas.

The DMM, DME and methanol conversions (X_i), and hydrogen productivity ($W(H_2)$) for the studied reactions were calculated using the following equations:

$$X_{DMM}(\%) = \frac{C_{DMM}^{in} - C_{DMM}^{out} \times C_{N_2}^{in}/C_{N_2}^{out}}{C_{DMM}^{in}} \times 100$$

$$X_{DME}(\%) = \frac{C_{DME}^{in} - C_{DME}^{out} \times C_{N_2}^{in}/C_{N_2}^{out}}{C_{DME}^{in}} \times 100$$

$$X_{Methanol}(\%) = \frac{C_{methanol}^{in} - C_{methanol}^{out} \times C_{N_2}^{in}/C_{N_2}^{out}}{C_{methanol}^{in}} \times 100$$

$$W(H_2) \left(\frac{l}{h \cdot g_{cat}} \right) = \frac{F \times C_{H_2} \times C_{N_2}^{in}/C_{N_2}^{out}}{100 \times m_{cat}}$$

where C^{in} , C^{out} are the inlet and outlet concentrations, F – total flow rate of the inlet reaction mixture (L/h), m_{cat} – catalyst weight (g).

The detection limits for CO, CO₂, H₂, DMM, DME, formaldehyde, methyl formate were 5×10^{-3} vol.% or better. The carbon imbalance in all catalytic experiments was below $\pm 3\%$.

3. Results and discussion

3.1. Catalyst characterization

Table 1 presents CuO and CeO₂ loadings, S_{BET} and concentrations of acid sites for the studied catalysts. For the CeO₂/γ-Al₂O₃, CuO/γ-Al₂O₃, and CuO–CeO₂/γ-Al₂O₃ catalysts, the calculated (according to preparation protocol) CeO₂ and CuO loadings slightly exceed the actual values obtained by chemical analysis. The most likely reason is that the γ-Al₂O₃ support absorbed lower volume of the aqueous solutions of cerium and copper salts. S_{BET} of these catalysts is lower by $\leq 20\%$ than that of γ-Al₂O₃ (200 m²/g). The acid sites on γ-Al₂O₃ are mainly of the Lewis type [29,30]. The LAS concentration is 600 μmol/g (Table 1). Note that insignificant amount of BAS (< 20 μmol/g) was detected on γ-Al₂O₃ (not shown in Table 1). No BAS were observed on CeO₂/γ-Al₂O₃, CuO/γ-Al₂O₃, and CuO–CeO₂/γ-Al₂O₃. The LAS concentration on these catalysts was much lower than on γ-Al₂O₃. In particular, the LAS concentration on CuO–CeO₂/γ-Al₂O₃ was 60 μmol/g. Thus, the concentration of acid sites on the surface of γ-Al₂O₃ reduced significantly after copper oxide and/or ceria loading. Nevertheless, LAS typical for γ-Al₂O₃ are present on the surface of all the studied catalysts.

Reducibility of fresh (i.e., as-synthesized) CeO₂/γ-Al₂O₃, CuO/γ-Al₂O₃, and CuO–CeO₂/γ-Al₂O₃ catalysts was investigated by means of H₂-TPR. Fig. 1 presents the obtained results. CeO₂/γ-Al₂O₃ (curve 1) was not reduced till the temperature of 350 °C. This is quite natural since the CeO₂ reduction takes place at temperatures above 400 °C [31]. The CuO/γ-Al₂O₃ catalyst (curve 2) exhibited two hydrogen uptake peaks – at 220 and 255 °C. According to [32] they can be attributed to reduction of small and large CuO particles on the γ-Al₂O₃ surface, respectively. In contrast to CuO/γ-Al₂O₃, the CuO–CeO₂/γ-Al₂O₃ catalyst (curve 3) demonstrated one broad hydrogen uptake peak with a maximum at 180 °C shifted towards the lower temperature region. Moreover, quantitative analysis of the H₂ uptake showed that complete reduction of CuO to Cu metal occurred in CuO/γ-Al₂O₃, while in CuO–CeO₂/γ-Al₂O₃ only ~90% of CuO was reduced to copper. These facts indicate that the CuO and CeO₂ particles interact on the γ-Al₂O₃ surface to produce a solid solution of copper and cerium oxides [31,33].

The catalysts were characterized by XRD. Fig. 2 shows the XRD patterns of fresh and used (i.e., after the catalytic experiment) catalysts. Table 2 presents the obtained data. Note that the XRD patterns

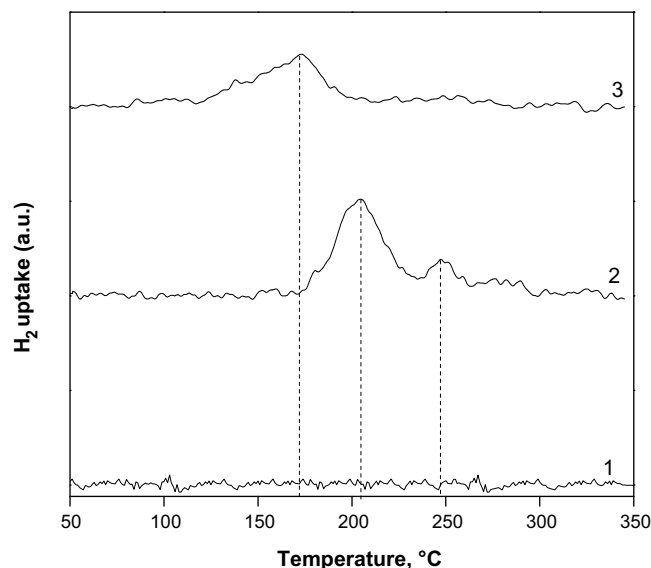


Fig. 1. H₂-TPR profiles of fresh CeO₂/γ-Al₂O₃ (1), CuO/γ-Al₂O₃ (2) and CuO–CeO₂/γ-Al₂O₃ (3) catalysts.

of the used (not shown in Table 2) and fresh CeO₂/γ-Al₂O₃ catalysts were the same. The XRD patterns of all samples contain diffraction peaks of γ-Al₂O₃, which consists of nanocrystalline particles (size ~5 nm) and has the unit cell parameter of 0.7924–0.7945 nm. In the case of fresh CuO/γ-Al₂O₃ and CuO–CeO₂/γ-Al₂O₃ catalysts, no copper oxide peaks were observed. This fact most likely means that CuO is present on γ-Al₂O₃ surface in the form of either amorphous or well dispersed species. The XRD patterns of the used CuO/γ-Al₂O₃ and CuO–CeO₂/γ-Al₂O₃ catalysts contained the peaks of copper metal with particle size 67 and 53 nm. This result seems to be quite natural, since the catalysts were exposed to reducing atmosphere. The fresh and used CeO₂/γ-Al₂O₃ and CuO–CeO₂/γ-Al₂O₃ catalysts exhibited diffraction peaks of CeO₂ (particle size 3.5–5 nm). The CeO₂ unit cell parameter (see Table 2) in the fresh and used CuO–CeO₂/γ-Al₂O₃ (0.5354 and 0.5389 nm, respectively) is lower than both the standard bulk value (0.5411 nm) and the value for CeO₂/γ-Al₂O₃ (0.5405 nm). According to [31,33,34], this fact indicates the formation of a mixed copper–cerium oxide (solid solution) due to insertion of Cu²⁺ into CeO₂ lattice.

The CuO–CeO₂/γ-Al₂O₃ catalyst was studied by TEM and EDX techniques. Fig. 3 shows the TEM images of the fresh and used

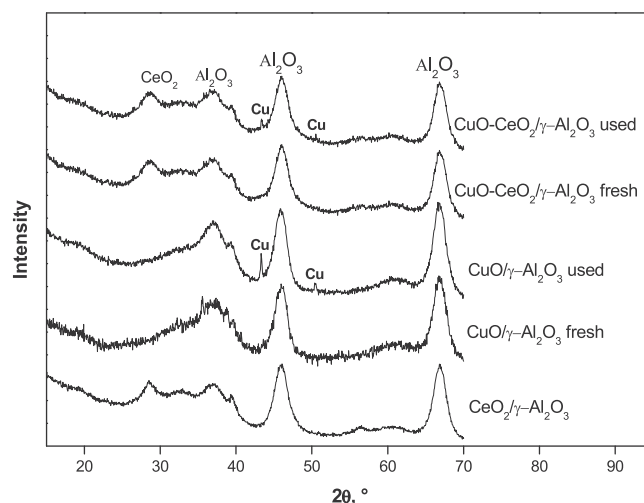


Fig. 2. XRD patterns of the catalysts.

Table 1
CuO and CeO₂ loading, S_{BET} and concentration of acid sites for the catalysts.

Catalyst	Loading (wt.%)				S_{BET} (m ² /g)	Concentration of LAS (μmol/g) ^a
	CuO Calculated	Actual	CeO ₂ Calculated	Actual		
γ-Al ₂ O ₃	–	–	–	–	200	600
CeO ₂ /γ-Al ₂ O ₃	–	–	5.0	4.4	170	200
CuO/γ-Al ₂ O ₃	10	9.3	–	–	170	90
CuO–CeO ₂ /γ-Al ₂ O ₃	10	9.3	5.0	4.4	160	60

^a LAS – Lewis acid sites.

Table 2
XRD data for the catalysts.

Catalyst	Phase composition	Unit cell parameters, nm		CSR (nm) ^a	
		a (CeO ₂)	D (CeO ₂)	D (Cu)	
5% CeO ₂ /γ-Al ₂ O ₃	(Fresh/used)	0.5405	5	–	
10% CuO/γ-Al ₂ O ₃	Fresh	–	–	–	
	Used	–	–	67	
10% CuO–5% CeO ₂ /γ-Al ₂ O ₃	Fresh	0.5354	4	–	
	Used	0.5389	3.5	53	

^a Size of coherent-scattering regions.

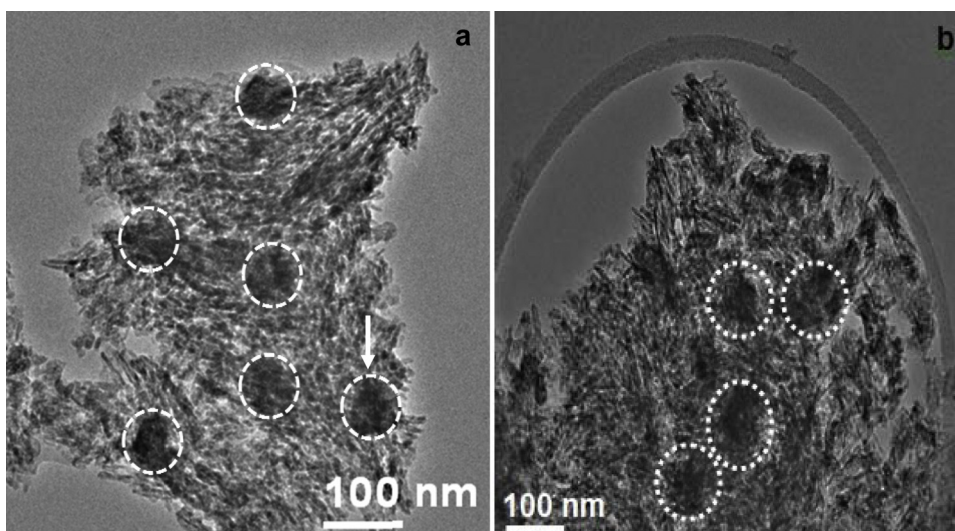


Fig. 3. TEM images of fresh (a) and used (b) CuO–CeO₂/γ-Al₂O₃ catalysts.

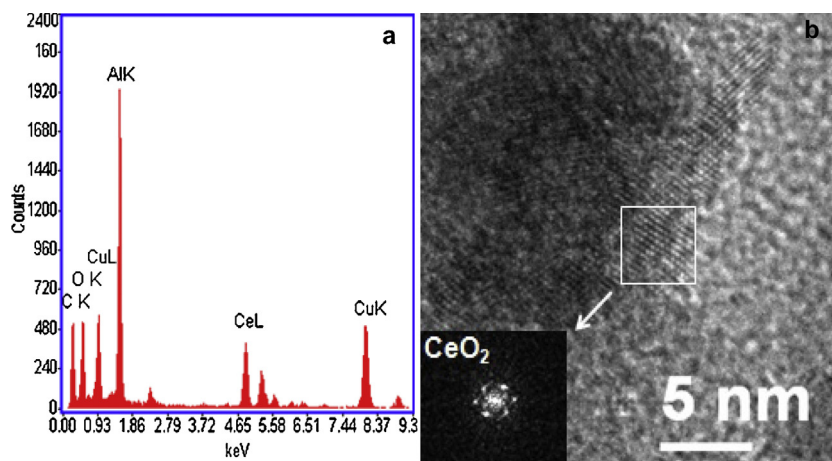


Fig. 4. EDX spectrum (a) and HRTEM image (b) of agglomerates in CuO–CeO₂/γ-Al₂O₃ catalyst marked with an arrow in Fig. 3a. Insert in b – Fourier diffractogram of the selected zone.

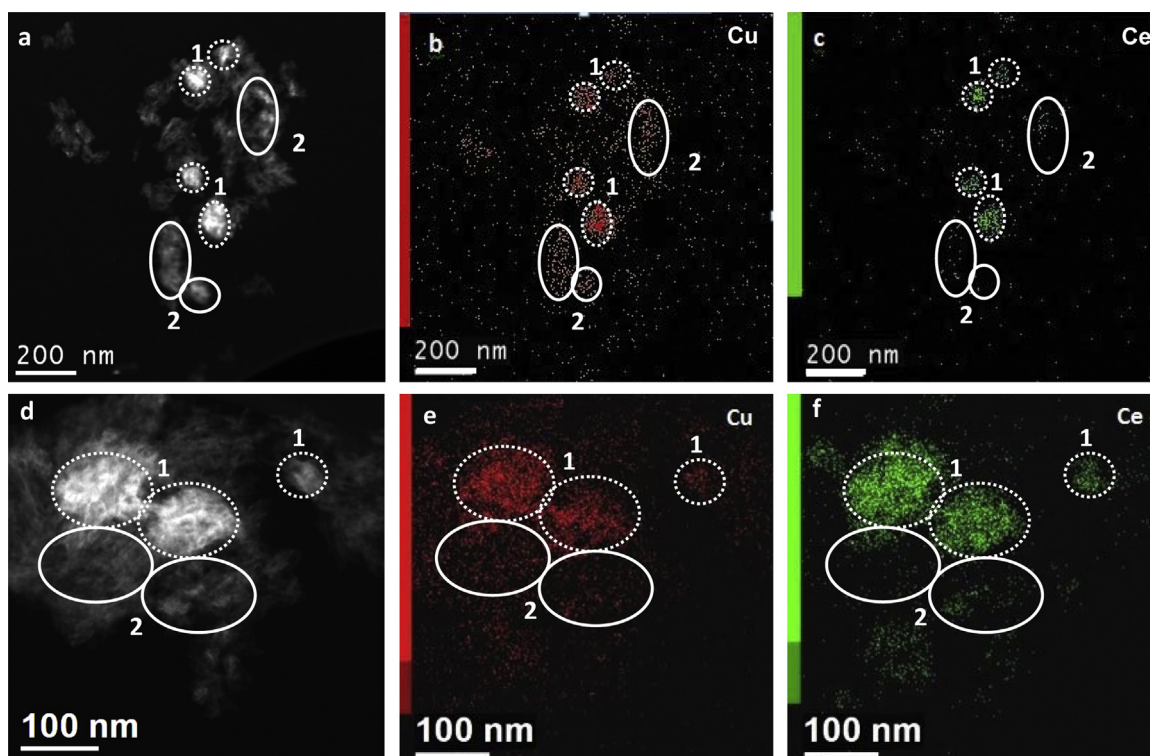


Fig. 5. STEM HAADF images and corresponding Cu and Ce mapping for fresh (a–c) and used (d–f) CuO–CeO₂/γ-Al₂O₃ catalysts. 1 – zone where Cu and Ce species are present simultaneously. 2 – zone where Cu predominates.

catalysts, which are obviously similar. Agglomerates (dark patches outlined by light circles) with the size of 80–100 nm are observed. The agglomerates were studied by EDX and HR TEM. Fig. 4 exemplifies the EDX spectrum and HR TEM image of the agglomerate in the CuO–CeO₂/γ-Al₂O₃ catalyst marked with an arrow in Fig. 3a. One can see that the agglomerate contains copper and cerium in atomic ratio Cu/Ce ~1/1 (Fig. 4a). The CeO₂ particles (interplanar distances $d_{(111)} = 0.312$ and $d_{(200)} = 0.271$ nm, Fig. 4b) are observed in the agglomerate. In general, the agglomerates in both fresh and used catalysts are compositionally inhomogeneous and contain copper and cerium in atomic ratio Cu/Ce = 1/1–2/1 (according to the EDXA data), as well as ceria particles (according to the HR TEM data). Copper-based particles were not identified by HR TEM, most likely, due to their low contrast.

HAADF-STEM is a good method for determining the surface elementary composition and compositional homogeneity of supported particles. Fig. 5 presents the HAADF-STEM images and copper–cerium mapping of the fresh and used CuO–CeO₂/γ-Al₂O₃ catalysts. Note that the HAADF-STEM image contrast becomes brighter as the atomic mass of the elements in the particle becomes heavier. This makes it possible to distinguish which elements are present. The HAADF-STEM images (Fig. 5a and d) of both catalysts are similar. The zones in Fig. 5 marked by number 1 correspond to agglomerates with the size of 80–100 nm containing both cerium and copper, in good agreement with the TEM data. The zones marked by number 2 correspond to areas with copper-based species.

Thus, the obtained data prove CuO–CeO₂/γ-Al₂O₃ to be a bifunctional catalyst. It contains:

- LAS of γ-Al₂O₃ (Table 1) which could be responsible for DMM hydration to methanol and formaldehyde;
- copper-containing species in the form of γ-Al₂O₃-supported copper-based particles and agglomerates containing both copper

and cerium (Figs. 3–5), which could be responsible for steam reforming of methanol and formaldehyde.

Most likely, the agglomerates are compact 80–100 nm particles (Figs. 3 and 5) consisting of CeO₂ nanoparticles, CuO–CeO₂ solid solution nanoparticles (see Table 2 and Fig. 4), and finely dispersed copper-based particles (judging by high Cu/Ce atomic ratio, see Fig. 4).

3.2. DMM steam reforming

3.2.1. Catalytic performance of γ-Al₂O₃ and CeO₂/γ-Al₂O₃

Under DMM SR conditions, the γ-Al₂O₃ and CeO₂/γ-Al₂O₃ samples catalyzed the DMM hydration (2). Methanol and formaldehyde were the main reaction products; neither hydrogen nor carbon oxides were detected. By-products (DME and methyl formate) appeared at temperatures above 225 °C in the amounts not exceeding 0.6 and 1.8 vol.%, respectively.

Fig. 6 shows the temperature dependencies of DMM conversion, and the CH₂O and CH₃OH outlet concentrations for DMM hydration over γ-Al₂O₃ and CeO₂/γ-Al₂O₃. It also presents the equilibrium values of DMM conversion and the CH₂O and CH₃OH concentrations calculated in the assumption that only DMM hydration (reaction (2)) takes place in the system. Obviously, both catalysts demonstrate similar dependencies. As the temperature increases from 150 to 300 °C, the DMM conversion and methanol concentration increase and reach equilibrium values. The formaldehyde concentration first increases and approaches the equilibrium value, then it decreases. The decrease in the formaldehyde concentration at temperatures above 225 °C for γ-Al₂O₃ and above 250 °C for CeO₂/γ-Al₂O₃ is due to the formaldehyde disproportionation to methyl formate (Tishchenko–Claisen reaction).

Compared to γ-Al₂O₃, the temperature dependencies of DMM conversion, and CH₂O and CH₃OH outlet concentrations for CeO₂/γ-Al₂O₃ are shifted to higher temperatures (Fig. 6). This fact

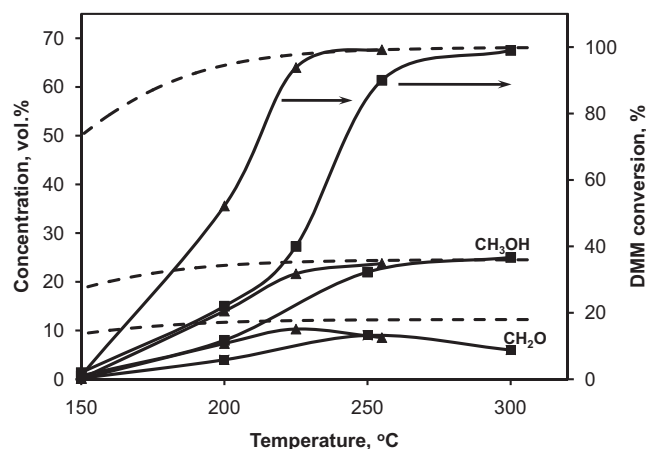


Fig. 6. Effect of temperature on DMM conversion, methanol and formaldehyde outlet concentrations in DMM hydration over $\gamma\text{-Al}_2\text{O}_3$ (▲) and $\text{CeO}_2/\gamma\text{-Al}_2\text{O}_3$ (■) catalysts. Reaction conditions: $P = 1$ atm, $\text{GHSV} = 10,000 \text{ h}^{-1}$; Inlet composition, vol.%: $\text{DMM}:\text{H}_2\text{O}:\text{N}_2 = 14:70:16$. Solid lines – experiment, dotted lines – thermodynamic equilibrium values.

proves that $\gamma\text{-Al}_2\text{O}_3$ has higher catalytic activity in DMM hydration than $\text{CeO}_2/\gamma\text{-Al}_2\text{O}_3$, because the LAS concentration on $\gamma\text{-Al}_2\text{O}_3$ decreases after the CeO_2 deposition on its surface (see Section 3.1, Table 1). Since LAS on the $\gamma\text{-Al}_2\text{O}_3$ surface may transform to BAS in the presence of steam [35], the issue which acid sites (LAS or BAS) are responsible for DMM hydration needs further investigation.

3.2.2. Catalytic performance of $\text{CuO}/\gamma\text{-Al}_2\text{O}_3$ and $\text{CuO-CeO}_2/\gamma\text{-Al}_2\text{O}_3$

In contrast to $\gamma\text{-Al}_2\text{O}_3$ and $\text{CeO}_2/\gamma\text{-Al}_2\text{O}_3$, the $\text{CuO}/\gamma\text{-Al}_2\text{O}_3$ and $\text{CuO-CeO}_2/\gamma\text{-Al}_2\text{O}_3$ catalysts were active in DMM SR. H_2 , CO_2 , CO and CH_3OH were the main reaction products. Formaldehyde and methyl formate appeared in trace amounts ($< 2 \times 10^{-2}$ vol.%). DME was observed at temperatures $> 280^\circ\text{C}$ in the amounts below 0.5 and 1.0 vol.% for $\text{CuO-CeO}_2/\gamma\text{-Al}_2\text{O}_3$ and $\text{CuO}/\gamma\text{-Al}_2\text{O}_3$, respectively. Note that during the first hour on stream, both catalysts demonstrated similar characteristics, namely, the product distribution and the hydrogen productivity. However, the $\text{CuO-CeO}_2/\gamma\text{-Al}_2\text{O}_3$ remained stable during the whole operation period, whereas $\text{CuO}/\gamma\text{-Al}_2\text{O}_3$ decayed within 8 h on-stream.

Fig. 7 presents the temperature dependencies of DMM conversion and the H_2 , CO_2 , CO and CH_3OH outlet concentrations during DMM SR over $\text{CuO-CeO}_2/\gamma\text{-Al}_2\text{O}_3$. The equilibrium values of DMM

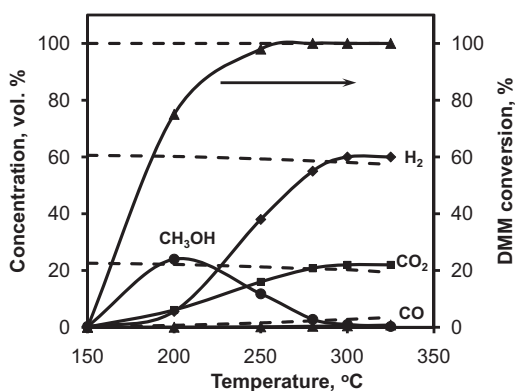


Fig. 7. Effect of temperature on DMM conversion and H_2 , CO , CO_2 and methanol outlet concentrations in DMM steam reforming over $\text{CuO-CeO}_2/\gamma\text{-Al}_2\text{O}_3$ catalyst. Reaction conditions: $P = 1$ atm, $\text{GHSV} = 10,000 \text{ h}^{-1}$; inlet composition, vol.%: $\text{DMM}:\text{H}_2\text{O}:\text{N}_2 = 14:70:16$. Solid lines – experiment, dotted lines – thermodynamic equilibrium values.

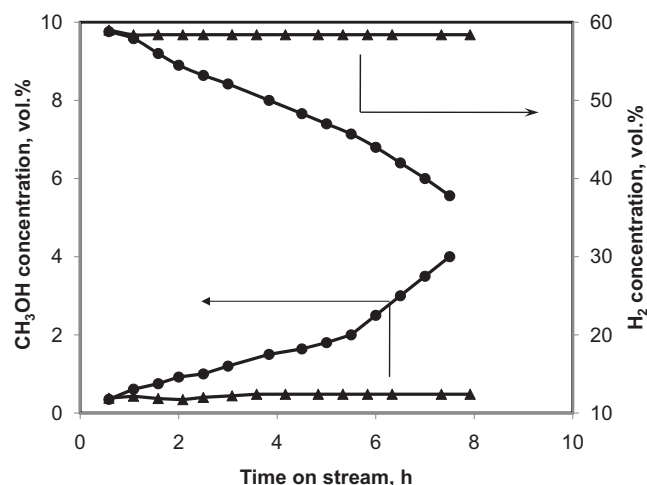


Fig. 8. Effect of time on stream on methanol and hydrogen outlet concentrations in DMM steam reforming over $\text{CuO}/\gamma\text{-Al}_2\text{O}_3$ (●) and $\text{CuO-CeO}_2/\gamma\text{-Al}_2\text{O}_3$ (▲) catalysts. Reaction conditions: $P = 1$ atm, $T = 280^\circ\text{C}$, $\text{GHSV} = 10,000 \text{ h}^{-1}$; Inlet composition, vol.%: $\text{DMM}:\text{H}_2\text{O}:\text{N}_2 = 14:70:16$.

conversion and product concentrations are shown as well. The equilibrium values were calculated in the assumption that DMM SR yielded CH_3OH , CH_2O , DME , H_2 , CO_2 and CO . The equilibrium concentrations of CH_3OH , CH_2O and DME were below 6×10^{-3} vol.% (not shown in Fig. 7).

Clearly, the DMM conversion increases with increasing temperature and reaches 100% at temperatures above 250°C . The methanol concentration passes through a maximum at 200°C and decreases to zero with further temperature increase. Such a behaviour is consistent with the suggested consecutive two-step reaction mechanism of DMM SR assuming the formation of methanol as an intermediate product (see reactions (2)–(4)). Methanol is formed by the DMM hydration reaction (2) on the acid sites of $\gamma\text{-Al}_2\text{O}_3$. Then it is consumed in the steam reforming reaction (3) that occurs on the Cu-containing species. It is essential that formaldehyde, which is also formed by reaction (2) and is an intermediate product, appears only in trace amounts. This observation does not contradict the DMM SR reaction mechanism and is explained by higher reactivity of formaldehyde in the steam reforming reaction compared to that of methanol [36].

The H_2 , CO_2 and CO outlet concentrations increase with increasing temperature (Fig. 7). At temperatures $\geq 300^\circ\text{C}$, the H_2 and CO_2 concentrations slightly exceed the equilibrium values, whereas the CO concentration (0.5 vol.%) remains below the equilibrium one. This is most likely related to the fact that H_2 and CO_2 are the primary products of reactions (3) and (4), while CO is formed by reaction (5). Obviously, if reaction (5) does not reach the equilibrium during the experiment, the H_2 and CO_2 concentrations should exceed the equilibrium values and the CO concentration should stay below it.

In general, the data shown in Fig. 7 prove that complete DMM conversion occurs in the temperature range of $300\text{--}325^\circ\text{C}$, and the main reaction products are H_2 , CO_2 and CO . Under these conditions, the hydrogen productivity reached the maximum value of $15.5 \text{ L H}_2/\text{g}_{\text{cat}}\cdot\text{h}$, the CO concentration remained below 0.5 vol.%.

Fig. 8 illustrates the effect of time on-stream on the outlet concentrations of methanol and hydrogen during DMM SR over $\text{CuO-CeO}_2/\gamma\text{-Al}_2\text{O}_3$ and $\text{CuO}/\gamma\text{-Al}_2\text{O}_3$ catalysts. The experiments were performed at 280°C , the inlet reaction mixture composition (vol.%) $\text{DMM}:\text{H}_2\text{O}:\text{N}_2 = 14:70:16$, and $\text{GHSV} = 10,000 \text{ h}^{-1}$. Under these conditions, both catalysts showed 100% DMM conversion; only traces of formaldehyde were detected. The CO and CO_2 concentrations were constant in the case of $\text{CuO-CeO}_2/\gamma\text{-Al}_2\text{O}_3$ and decreased with time in the case of $\text{CuO}/\gamma\text{-Al}_2\text{O}_3$.

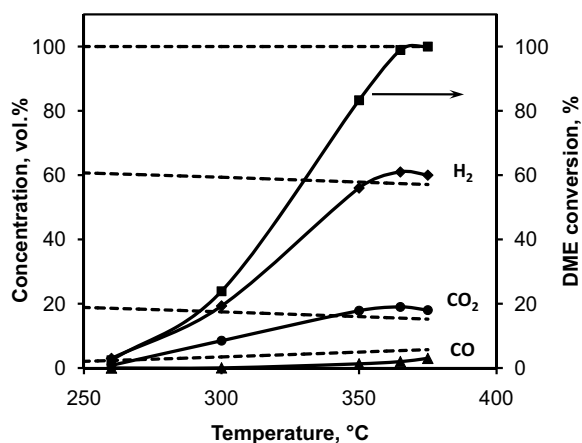


Fig. 9. Effect of temperature on DME conversion and H_2 , CO , CO_2 outlet concentrations in DME steam reforming over $CuO-CeO_2/\gamma-Al_2O_3$ catalyst. Reaction conditions: $P=1$ atm, $GHSV=10,000\ h^{-1}$; inlet composition, vol.%: $DME:H_2O:N_2=20:60:20$. Solid lines – experiment, dotted lines – thermodynamic equilibrium values.

One can see (Fig. 8) that during the first hour on-stream, the methanol and hydrogen concentrations were similar for both catalysts. In the case of $CuO-CeO_2/\gamma-Al_2O_3$, the concentrations of methanol and hydrogen remained constant during at least 8 h on-stream. In the case of $CuO/\gamma-Al_2O_3$, the methanol concentration increased from 0.4 to 4 vol.%, while the hydrogen concentration decreased from 60 to 40 vol.% after 8 h on-stream. In our view, these data mean that the acid sites of $\gamma-Al_2O_3$ (see Table 1 and Sections 3.1 and 3.2.1) responsible for DMM hydration are stable in both catalysts. The Cu-containing species responsible for methanol/formaldehyde SR are stable in $CuO-CeO_2/\gamma-Al_2O_3$ and lose activity in $CuO/\gamma-Al_2O_3$. As a result, the latter catalyst shows increasing methanol outlet concentration and decreasing hydrogen outlet concentration with increasing time on-stream.

According to temperature-programmed oxidation runs, the amount of carbon deposited on $CuO/\gamma-Al_2O_3$ catalyst during the reaction (~8 h on-stream) was ~0.05 wt.%, not exceeding the carbon content in the fresh catalyst. It is unlikely that carbonaceous deposits caused the catalyst deactivation. The XRD study showed (Section 3.1) the presence of well dispersed or amorphous Cu-containing species in fresh $CuO/\gamma-Al_2O_3$, whereas the used catalyst contained copper metal particles of size 67 nm. This observation means that copper sintering is the likely cause for the catalyst deactivation.

Taking into account the data presented in Section 3.1, we think that the activity and stability of the $CuO-CeO_2/\gamma-Al_2O_3$ catalyst in DMM SR is determined by copper–cerium oxide species (probably, $CuO-CeO_2$ solid solution nanoparticles and/or finely dispersed Cu-based particles) in alumina-supported copper–cerium oxide agglomerates. Note in this regard that, as shown in works [7–9], high activity and stability of CeO_2 -promoted Cu-containing catalysts in methanol SR is most likely attributed to the formation of stable highly dispersed copper species owing to metal (Cu) – support (CeO_2) interactions.

3.3. Steam reforming of DME and methanol over $CuO-CeO_2/\gamma-Al_2O_3$

According to the literature data, copper–ceria-based systems are active in DME SR [13,14] and methanol SR [7–9,14]. $CuO-CeO_2/\gamma-Al_2O_3$ is not an exception and shows activity for these reactions yielding H_2 , CO_2 and CO as the main products.

Figs. 9 and 10 demonstrate the temperature dependencies of DME and methanol conversions, and the H_2 , CO_2 and CO outlet

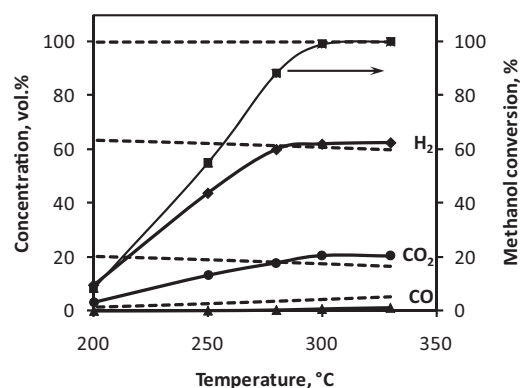


Fig. 10. Effect of temperature on methanol conversion and H_2 , CO_2 , and CO outlet concentrations in methanol steam reforming over $CuO-CeO_2/\gamma-Al_2O_3$ catalyst. Reaction conditions: $P=1$ atm, $GHSV=10,000\ h^{-1}$; inlet composition, vol.%: $CH_3OH:H_2O:N_2=40:40:20$. Solid lines – experiment, dotted lines – thermodynamic equilibrium values.

concentrations for DME SR and methanol SR over the $CuO-CeO_2/\gamma-Al_2O_3$ catalyst. The equilibrium values of the DME and methanol conversions and product concentrations are shown as well. The equilibrium values were calculated assuming H_2 , CO_2 and CO as the products of methanol SR, and H_2 , CO_2 , CO and methanol as the products of DME SR. The equilibrium concentration of methanol was below $\sim 6 \times 10^{-3}$ vol.% (not shown in Fig. 9).

Clearly, the conversions and the outlet H_2 , CO_2 , CO concentrations during both reactions increase with increasing temperature (Figs. 9 and 10). In the case of DME SR at temperatures above $365^\circ C$, the DME conversion reaches the equilibrium value ($\sim 100\%$), the H_2 and CO_2 outlet concentrations slightly exceed the equilibrium value, while the CO outlet concentration (~ 1 vol.%) remains below the equilibrium value (Fig. 9). Methanol SR demonstrates essentially a similar behaviour (Fig. 10) at temperatures above $275^\circ C$. The methanol conversion reaches the equilibrium value ($\sim 100\%$), the H_2 and CO_2 outlet concentrations slightly exceed the equilibrium value, the CO outlet concentration (~ 0.7 vol.%) remains below the equilibrium value. Such a behaviour results from the fact that both during DME SR and methanol SR H_2 and CO_2 are the primary products of reaction (3), whereas CO is formed by reaction (5). To avoid confusion, note that methanol in DME SR is formed by DME hydration. Obviously, if during the experiment the equilibrium of reaction (5) is not reached, the H_2 and CO_2 concentrations may exceed their respective equilibrium values, while the CO concentration may remain below it. Essentially a similar situation is observed in the case of DMM SR (see Section 3.2.2, Fig. 7).

Thus, the obtained data (Figs. 9 and 10) demonstrate that $CuO-CeO_2/\gamma-Al_2O_3$ is an efficient catalyst for DME SR and methanol SR to produce hydrogen-rich gas with low CO content (≤ 1.0 vol.%). In particular, during DME SR at $\sim 365^\circ C$ and methanol SR at $\sim 300^\circ C$, the DME and methanol conversions were close to 100%, with hydrogen productivity reaching $\sim 15\ L\ H_2/(g_{cat}\cdot h)$ or $\sim 0.6\ mol\ H_2/(g_{cat}\cdot h)$.

As reported in literature, performance of $CuO-CeO_2$ based catalysts in DME SR [13,14] and methanol SR [7–9,14] was studied under experimental conditions similar to those in the present work. It was reasonable to compare the obtained results with the literature data. According to [13,14], alumina-supported $CuO-CeO_2$ catalysts in DME SR at $350^\circ C$ provided a $\sim 100\%$ DME conversion, hydrogen productivity of ~ 0.4 – $0.6\ mol\ H_2/(g_{cat}\cdot h)$ and low CO content in the hydrogen-rich gas. These data are obviously similar to the result on DME SR reported in the present work (Fig. 9). According to [7–9,14], the $CuO-CeO_2$ based catalysts in methanol SR provided at $250^\circ C$ a 80–90% methanol conversion, hydrogen productivity of ~ 0.35 – $0.50\ mol\ H_2/(g_{cat}\cdot h)$ and low CO content in the hydrogen-rich gas. In the present work, the $CuO-CeO_2/\gamma-Al_2O_3$

Table 3
Performance of bifunctional CuO–CeO₂/γ-Al₂O₃ catalyst in DMM, DME and methanol steam reforming to hydrogen-rich gas. Reaction conditions: *P* = 1 atm, GHSV = 10,000 h^{−1}.

Reaction	Inlet composition (vol.%)	<i>T</i> (°C)	Concentration (vol.%)		H ₂ productivity, L H ₂ /(h g _{cat})
			H ₂	CO	
DMM SR	DMM:H ₂ O:N ₂ = 14:70:16	300	59.4	0.5	15.5
DME SR	DME:H ₂ O:N ₂ = 20:60:20	365	60	1	15
Methanol SR	CH ₃ OH:H ₂ O:N ₂ = 40:40:20	300	61.5	0.7	15

catalyst provided at 250 °C a ~60% methanol conversion, hydrogen productivity of ~0.37 mol H₂/(g_{cat}·h) and low CO content in the hydrogen-rich gas (Fig. 10). Clearly, the obtained results and the literature data on methanol SR are similar.

So, the catalytic behaviour of the CuO–CeO₂ based systems in DME SR and methanol SR reported in this work and in the literature is almost the same.

3.4. Comparative analysis of CuO–CeO₂/γ-Al₂O₃ catalyst behaviour in DMM, DME and methanol SR: a multi-fuel processor approach

As it is shown in Sections 3.2 and 3.3, CuO–CeO₂/γ-Al₂O₃ is quite an active catalyst for DMM, DME and methanol steam reforming reactions. To estimate the catalyst feasibility for multi-fuel processor applications (i.e., generation of hydrogen-rich gas from various feed-stocks over the same catalyst under similar reaction conditions), it seemed reasonable to compare its performance in DMM, DME and methanol steam reforming.

Table 3 presents the required comparative data (see Figs. 7, 9 and 10): temperature of almost complete conversion of DMM, DME and methanol yielding H₂, CO₂ and CO as the main products; H₂ and CO concentrations in the obtained hydrogen-rich gas; hydrogen productivity. Complete conversion of DMM, DME and methanol was reached at 300, 365 and 300 °C, respectively. Regardless of the feedstock type, the catalyst yielded gas mixtures with similar H₂ concentrations (~60 vol.%) and low CO content (<1 vol.%). The latter fact is important as it allows using of a simpler scheme for production of hydrogen-rich gas for fuel cell application that dictates strict requirements regarding the CO impurity. Indeed, the hydrogen-rich gas produced by DMM, DME, and methanol SR can be used for direct feeding of HT PEM FC without any further CO removal [1]. For LT PEM FC feeding, the hydrogen-rich gas should be purified of CO to the level of 10 ppm [2], which can be achieved by selective oxidation [37,38] or methanation [39] of CO, bypassing the stage of the water-gas shift reaction.

Hydrogen productivity of CuO–CeO₂/γ-Al₂O₃ (Table 3) in DME, DMM and methanol SR reactions is almost the same ~15 L H₂/g_{cat}·h. So, 50 g of the catalyst is sufficient to provide operation of a 1 kW PEMFC-based power unit using any substrate – DMM, DME or methanol – as the primary fuel.

Thus, the CuO–CeO₂/γ-Al₂O₃ bifunctional catalyst is quite efficient for DMM, DME and methanol SR and is very high promising for development of a multi-fuel processor for reforming of all three type fuels over the same catalyst under similar reaction conditions into hydrogen-rich gas with low CO content appropriate for FC feeding applications.

4. Conclusions

Bifunctional CuO–CeO₂/γ-Al₂O₃ catalyst containing on its surface both acidic and copper-based sites is active and selective for DMM SR to hydrogen-rich gas with low (<1 vol.%) CO content. In particular, the developed catalyst provides for 100% DMM conversion with hydrogen production rate of ca. 15.5 L H₂/(g_{cat}·h) at GHSV = 10,000 h^{−1} and *T* = 300 °C. It is very promising

for implementation of a multi-fuel processor approach as it enables production of hydrogen-rich gas from more than one fuel (DMM, DME and methanol) under similar reaction conditions. Moreover, the produced hydrogen-rich gas can be used for direct feeding of HT PEM FC. After CO removal by CO PROX or selective CO methanation, it can be used in LT PEM FC. These factors will obviously help to simplify the fuel processor designs, and improve the technology cost-efficiency.

Acknowledgements

The authors are grateful to Dr. O.A. Bulavchenko for assistance in XRD experiments and Dr. O.A. Stonkus for performing TEM/EDX and STEM-HAADF analysis.

This work was partially supported by the Council for Grants of the President of the Russian Federation for State Support of Young Russian Scientists (Grant no. MK.2199.2013.3), by the RFBR Grant no. 14-03-00457-a and by the Ministry of Education and Science of the Russian Federation.

References

- [1] S.J. Peighambari, S. Rowshanzamir, M. Amjadi, Int. J. Hydrogen Energy 35 (2010) 9349–9384.
- [2] A. Chandan, M. Hattenberger, A. El-kharouf, S. Du, A. Dhir, V. Self, B.G. Pollet, A. Ingram, W. Bujalski, J. Power Sources 231 (2013) 264–278.
- [3] V. Mehta, J.S. Cooper, J. Power Sources 114 (2003) 32–53.
- [4] M. O'Connell, G. Kolb, K.-P. Schelhaas, M. Wichert, D. Tiemann, H. Pennemann, R. Zapf, Chem. Eng. Res. Des. 90 (2012) 11–18.
- [5] A. Iulianelli, P. Riberinha, A. Mendes, A. Basile, Renew. Sust. Energy Rev. 29 (2014) 355–368.
- [6] S.D. Jones, H.E. Hagelin-Weaver, Appl. Catal. B 90 (2009) 195–204.
- [7] Y. Liu, T. Hayakawa, T. Tsunoda, K. Suzuki, S. Hamakawa, K. Murata, R. Shiozaki, T. Ishii, M. Kumagai, Top. Catal. 22 (2003) 205–213.
- [8] H. Oguchi, T. Nishiguchi, T. Matsumoto, H. Kanai, K. Utani, Y. Matsumura, S. Imamura, Appl. Catal. A 281 (2005) 69–73.
- [9] X. Zhang, P. Shi, J. Mol. Catal. A: Chem. 194 (2003) 99–105.
- [10] J. Vicente, A.G. Gayubo, J. Erena, A.T. Aguayo, M. Olazar, J. Bilbao, Appl. Catal. B 130–131 (2013) 73–83.
- [11] T.A. Semelsberger, K.C. Ott, R.L. Borup, H.L. Greene, Appl. Catal. A 309 (2006) 210–223.
- [12] S.D. Badmaev, G.G. Volkova, V.D. Belyaev, V.A. Sobyenin, React. Kinet. Catal. Lett. 90 (2007) 205–211.
- [13] G. Volkova, S. Badmaev, V. Belyaev, L. Plyasova, A. Budneva, E. Paukshtis, V. Zaikovskiy, V. Sobyenin, Stud. Sur. Sci. Catal. 167 (2007) 445–450.
- [14] P.V. Snytnikov, S.D. Badmaev, G.G. Volkova, D.I. Potemkin, M.M. Zyryanova, V.D. Belyaev, V.A. Sobyenin, Int. J. Hydrogen Energy 37 (2012) 16388–16396.
- [15] J. Ereña, J. Vicente, A.T. Aguayo, M. Olazar, J. Bilbao, A.G. Gayubo, Appl. Catal. B 142–143 (2013) 315–322.
- [16] N. Shimoda, H. Muroyama, T. Matsui, K. Faungnawakij, R. Kikuchi, K. Eguchi, Appl. Catal. A 409–410 (2011) 91–98.
- [17] X. Lu, Z. Qin, M. Dong, H. Zhu, G. Wang, Y. Zhao, W. Fan, J. Wang, Fuel 90 (2011) 1335–1339.
- [18] <http://huayan-formaldehyde.com/methylal.html>
- [19] N.P. Cheremisinoff, Industrial Solvents Handbook, CRC Press, New York, 2003.
- [20] J. Lojewski, J. Wasilewski, K. Terelak, T. Łojewski, A. Kołodziej, Catal. Commun. 9 (2008) 1833–1837.
- [21] G.K.S. Prakash, M.C. Smart, G.A. Olah, S.R. Narayanan, W. Chun, S. Surampudi, G. Halpert, J. Power Sources 173 (2007) 102–109.
- [22] R. Zhu, X. Wang, H. Miao, X. Yang, Z. Huang, Fuel 90 (2011) 1731–1737.
- [23] Q. Sun, A. Auroux, J. Shen, J. Catal. 244 (2006) 1–9.
- [24] Y. Fu, J. Shen, J. Catal. 248 (2007) 101–110.
- [25] H. Shen, Y. Fu, Q. Sun, S. Zuo, A. Auroux, J. Shen, Catal. Commun. 9 (2008) 801–806.
- [26] S.D. Badmaev, A.A. Pechenkin, V.D. Belyaev, S.A. Venyaminov, P.V. Snytnikov, V.A. Sobyenin, V.N. Parmon, Doklady Phys. Chem. 452 (2013) 251–253.
- [27] E.A. Paukshtis, IR Spectroscopy for Heterogeneous Acid-Base Catalysis, Nauka, Novosibirsk, 1992.

- [28] G.G. Volkova, L.M. Plyasova, L.N. Shkuratova, A.A. Budneva, E.A. Paukshtis, M.N. Timofeeva, V.A. Likhonobov, *Stud. Surf. Sci. Catal.* 147 (2004) 403–408.
- [29] J. Shen, M.J. Lochhead, K.L. Bray, Y. Chen, J.A. Dumesic, *J. Phys. Chem.* 99 (1995) 2384–2392.
- [30] S.D. Badmaev, V.D. Belyaev, G.G. Volkova, E.A. Paukshtis, V.A. Sobyenin, *React. Kinet. Catal. Lett.* 90 (2007) 197–204.
- [31] T. Caputo, L. Lisi, R. Pirone, G. Russo, *Appl. Catal. A* 348 (2008) 42–53.
- [32] M.-F. Luo, P. Fang, M. He, Y.-L. Xie, *J. Mol. Catal. A: Chem.* 239 (2005) 243–248.
- [33] X. Jiang, L. Lou, Y. Chen, X. Zheng, *J. Mol. Catal. A: Chem.* 197 (2003) 193–205.
- [34] U. Menon, H. Poelman, V. Bliznuk, V.V. Galvita, D. Poelman, G.B. Marin, *J. Catal.* 295 (2012) 91–103.
- [35] T. Takeguchi, K.-I. Yanagisawa, T. Inui, M. Inoue, *Appl. Catal. A* 192 (2000) 201–209.
- [36] N. Takezawa, N. Iwasa, *Catal. Today* 36 (1997) 45–56.
- [37] D. Gamarra, A. López Cámara, M. Monte, S.B. Rasmussen, L.E. Chinchilla, A.B. Hungria, G. Munuera, N. Gyorffy, Z. Schay, V. Cortés Corberán, J.C. Conesa, A. Martínez-Arias, *Appl. Catal. B* 130–131 (2013) 224–238.
- [38] P.V. Snytnikov, D.I. Potemkin, E.V. Rebrov, V.A. Sobyenin, V. Hessel, J.C. Schouten, *Chem. Eng. J.* 160 (2010) 923–929.
- [39] M.M. Zyryanova, P.V. Snytnikov, Y.I. Amosov, V.A. Kuzmin, V.A. Kirillov, V.A. Sobyenin, *Chem. Eng. J.* 176 (2011) 106–113.